Available online at www.sciencedirect.com
SCIENCE DIRECT®
Sensors and Actuators B 102 (2004) 107–116
SENSORS AND ACTUATORS B CHEMICAL
www.elsevier.com/locate/snb

Fluorescence-based optical sensor design for molecularly imprinted polymers

Yin-Chu Chen [a], Jennifer J. Brazier [b], Mingdi Yan [b], Paulo R. Bargo [a], Scott A. Prahl [a,*]

[a] *Biomedical Engineering Department, Oregon Health and Science University, Portland, OR 97225, USA*
[b] *Department of Chemistry, Portland State University, Portland, OR, USA*

Received 25 August 2003; accepted 20 February 2004

Available online 22 July 2004

Abstract

A Monte Carlo model was developed to analyze the sensitivity and the performance of a fluorescence-based molecularly imprinted polymer (MIP) sensor. The MIP sensor consisted of highly cross-linked polyurethane containing anthracene binding sites coated on a transparent substrate. The optical properties of MIPs, the quantum yields of anthracene within MIPs, and the fluorescence of MIPs were measured. The rebinding capacity of the MIPs was about 1 μmol/g or roughly seven times binding rate of non-imprinted polymers. The MIP fluorescence emission at 404 nm was measured for thicknesses ranging from 100 to 2000 μm containing templated anthracene concentrations ranging from 60 to 600 ppm for excitation at 358 nm. The emission agreed with model predictions within 15%. This sensing system could only distinguish anthracene down to 15 ppm due to fluorescence from the polymer matrix. To make a fluorescence-based MIP sensor that is capable of detecting one part per billion analyte concentration with a 200 μm thick MIP film, our model suggests that imprinted polymers would need to have an absorption coefficient less than 0.001 cm^{-1}, or have a quantum yield 10^5 times lower than that of the analyte at the detection wavelength.

Keywords: Fluorescence sensor; Monte Carlo model; Imprinted polyurethane; Anthracene

1. Introduction

Biochemical sensors are used in clinical diagnostics, the pharmaceutical industry, environmental pollutant monitoring, food analysis, and detection of biological warfare agents. A biochemical sensor incorporates a biochemical recognition element along with a physical or chemical transducer. The recognition element must be specific to the target analyte and stable in a wide variety of environments. Recognition elements using immunosensors (e.g., antibodies) have excellent specificity and sensitivity [1–6], but require specific antibody synthesis, may have sterilization problems, and may suffer from stability issues [7,6]. Various biomimetic sensors that alleviate one or more of these drawbacks have been developed [8–10]. In this paper, sensors based on molecularly imprinted polymers (MIPs) are examined.

The recognition properties of MIPs arise from the way they are prepared. During synthesis, functional and cross-linking monomers are copolymerized in the presence of a target analyte (the imprinted molecule) that acts as a molecular template. The monomers are chosen for their ability to interact with the functional groups of the template molecule. Polymerization/cross-linking yields a network polymer with the template molecules incorporated. After the extraction of template molecules, the resulting cavities retain their "memory" for the target analyte [9]. MIPs are robust, stable, and resistant to a wide range of pH, humidity, and temperature [11]. MIPs are also relatively inexpensive to produce and can be synthesized for analytes for which no natural antibody exists [12].

Several groups have integrated MIPs with optical fibers [13,14] or waveguides [15–17]. Dickert et al. [15,17] used a quartz planar waveguide coated with a several-micron thick layer of MIP imprinted with various fluorescent polyaromatic hydrocarbons. Fluorescence emission of trapped analytes in the polymer matrix was used to detect analyte concentrations down to several μg/l [18,15,19].

To create practical sensing devices, the complex interplay of the factors affecting detection needs to be understood. Some studies have attempted to build a theoretical model for the sensitivity of an optical sensor [20–22]. A ray optics

* Corresponding author. Tel.: +1-503-216-2197.
E-mail address: prahl@bme.ogi.edu (S.A. Prahl).

0925-4005/$ – see front matter © 2004 Elsevier B.V. All rights reserved.
doi:10.1016/j.snb.2004.02.044

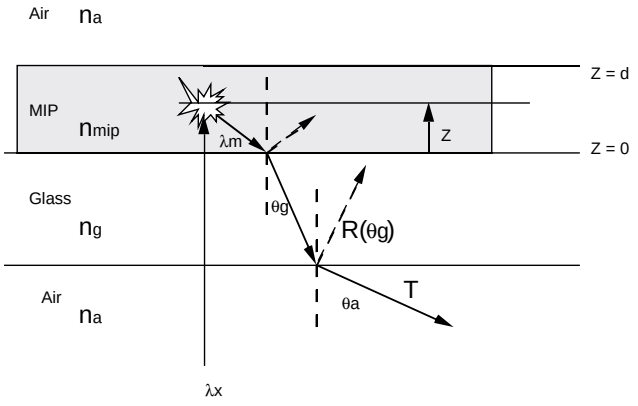

Fig. 1. The schematic representation of light path of our sensing system consisting of MIP coated on the flat bottom of a glass vial.

model was used to calculated to the detection limit of a total internal reflection fluorescence (TIRF)-sensing system [20,21]. Although ray optics method might provide some accuracy for TIRF spectrometry [20,21], the equation derived was an approximation and is limited to a particular sensor design. In this work, we examined three issues that affect the sensitivity of a fluorescence-based MIP sensor: the fluorescence collection efficiency, the optical properties of the MIP, and the rebinding performance of the MIP. With further analysis, we are able to select optimal design parameters for a MIP sensor. The optical properties of the MIP samples were measured to provide the background information for the theoretical model. The absorption coefficient, the refractive index, and the fluorescence quantum efficiency of the MIPs were measured while the original template molecules were still present in the matrix. The effects of the thickness of the MIP film, the background absorption, and the background fluorescence on the sensor sensitivity were analyzed theoretically in a Monte Carlo simulation. Finally, the rebinding capacities of the imprinted polymers were examined by extracting the original template molecules from the polymer matrix and subsequently measuring the rebound analyte concentrations when polymer samples were exposed to the analyte solutions.

2. Theoretical model

Our sensor consists of a layer of MIP on a transparent substrate. Fig. 1 illustrates the schematic representation of the light path. The excitation was perpendicular to the layer surface and the emission was collected on the same side as the excitation. The absorption coefficients of MIPs at the excitation and emission wavelength were $\mu^{x}_{urethane}$ and $\mu^{m}_{urethane}$, and the absorption coefficient of anthracene was $\mu^{x}_{anthracene}$ at the excitation wavelength. The refractive indices of MIPs, glass plate and air were n_{mip}, n_g and n_a, respectively. For simplicity, all elements were assumed homogeneous and isotropic.

In our Monte Carlo model, excitation photons were launched normally to the MIP layer. The photons were propagated, according to Beer's law, a random distance S^x to the depth at which they were absorbed ($S^x = -\ln(\xi/(\mu^x_{urethane} + \mu^x_{anthracene}))$, where ξ is a random number uniformly distributed between 0 and 1). The fraction of photons absorbed by the polyurethane was $\mu^x_{urethane}/(\mu^x_{urethane} + \mu^x_{anthracene})$ and the fraction absorbed by anthracene was $\mu^x_{anthracene}/(\mu^x_{urethane} + \mu^x_{anthracene})$. Both produced fluorescent light with different quantum yields, $\Phi^{404}_{urethane}$ for polyurethane and $\Phi^{404}_{anthracene}$ for anthracene. Fluorescent photons were emitted uniformly in all directions. The emission photons had three possible fates: (1) to be absorbed by polyurethane, (2) to be reflected at the MIP-glass boundary, or (3) to propagate through MIPs to the glass plate. The conditions for reflection depended on the unpolarized Fresnel reflection at the particular angle of incidence [23]. Photons entering the glass were either reflected at the glass–air boundary or transmitted into the air (which again depended on the Fresnel reflection). Photon paths were corrected for refraction angles at all boundaries. Finally, those fluorescent photons transmitted from the MIPs through the glass go into the air. Only some proportion of these transmission photons can be collected by the concave mirror, reflected by the mirror, and then sent to the sensing system (see Fig. 2). These fractions were all counted into the geometry factor, G, since this depends on the geometry of the setup, and the relative positions of the mirrors in the fluorimeter. Fluorescent photons arising from polymer $N^m_{urethane}$ or anthracene $N^m_{anthracene}$ were recorded separately. With total of N^x_{model} excitation photons launched in the model, the fluorescence collection efficiency E_f was

$$E_f = \frac{\Phi^{404}_{urethane} N^m_{urethane} + \Phi^{404}_{anthracene} N^m_{anthracene}}{N^x_{model}} G \quad (1)$$

E_f represents the ratio of the collected fluorescence photons to the input excitation photons. The value of E_f is between 0 and 1. Experimentally, E_f was equal to I^{404}_{mip}/I^x_{exp}, where I^{404}_{mip} is the emission from MIPs at 404 nm and I^x_{exp} the absorbed excitation light. If I^{404}_{mip}/I^x_{exp} is equal to Eq. (1), then

$$\frac{I^{404}_{mip}}{I^x_{exp} G} = \frac{\Phi^{404}_{urethane} N^m_{urethane} + \Phi^{404}_{anthracene} N^m_{anthracene}}{N^x_{model}} \quad (2)$$

Since G was unknown, and difficult to be determined accurately, we calculated the term, $I^x_{exp}G$, by comparing the result of the Monte Carlo simulation with the experimental result of the fluorescence emission of a standard anthracene cyclohexane solution. The simulation of anthracene cyclohexane solutions in a quartz cuvette was the same as the simulation described above, except we replaced MIPs by cyclohexane solutions. If N^m_{std} is the total emission photons from the standard solution and Φ_{std} is the quantum yield of the standard solution, then the theoretical fluorescence collection efficiency for the standard solution E_{std} is $\Phi_{std} N^m_{std} G/N^x_{model}$. Again, experimentally, E_{std} is equal to I^m_{std}/I^x_{exp}, where I^m_{std}

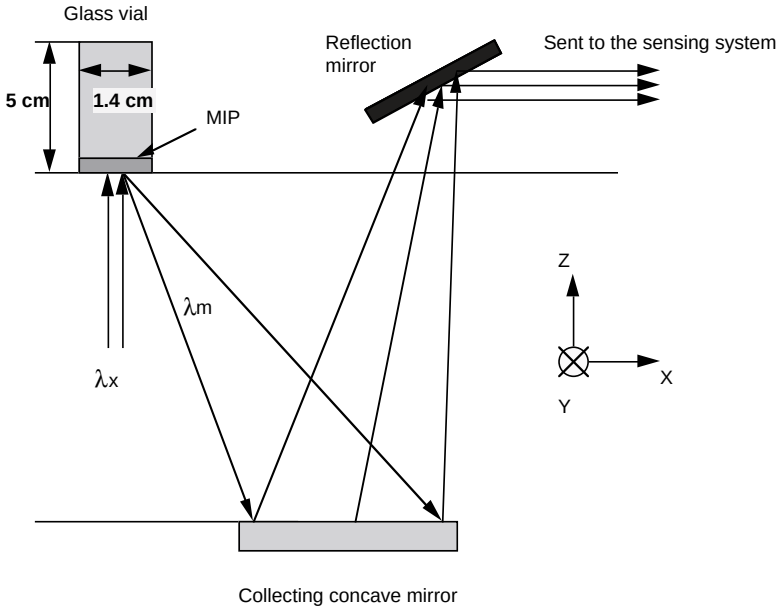

Fig. 2. The optical setup of MIP fluorescence measurement consists of a glass container (diameter = 1.4 cm, height = 5 cm) coated with MIPs as the sensing layer on the flat bottom and a collecting concave mirror. As shown here, only some proportions of the emission λ_m can be collected by the concave mirror, reflected by the mirror, and then sent to the sensing system. These proportions are all counted into the geometry factor, G.

is the total emission of the standard solution measured experimentally. Therefore,

$$\frac{I^{m}_{std}}{I^{x}_{exp}G} = \frac{\Phi_{std}N^{m}_{std}}{N^{x}_{model}} \quad (3)$$

Since $N^{m}_{std}/N^{x}_{model}$ can be calculated from the model, I^{m}_{std} can be measured from the experiment, and Φ_{std} is known, $I^{x}_{exp}G$ can then be calculated and substituted into Eq. (2).

In our simulations, the following values were used. The background absorption coefficients of cyclohexane, $\mu^{x}_{cyclohexane}$ and $\mu^{m}_{cyclohexane}$, were assumed to be 0.01 cm^{-1}, while the absorption coefficient of MIPs was 15 cm^{-1} for excitation and 3.5 cm^{-1} for emission (see Section 4). The refractive index of MIP n_{mip}, cyclohexane $n_{cyclohexane}$, the quartz cuvette n_q, and the glass vial n_g were 1.47, 1.43, 1.47, and 1.54 respectively. Two million photons were launched for each simulation set. Two free parameters, the thickness of the sensing layer t, and the concentration-dependent absorption coefficient of anthracene, $\mu^{x}_{anthracene}$, were varied. Finally, we compared the model results, the right hand side of Eq. (2), with the experimental results, the left hand side of Eq. (2).

3. Materials and methods

3.1. Materials

Bisphenol A, phloroglucinol, and anthracene were purchased from Aldrich and were used as received. A mixture of p,p'-diisocyanatodiphenylmethane and 30% p,o,p'-triisocyanatodiphenylmethane was purchased from Merck-Schuchardt (Hohenbrunn, Germany) and stored under nitrogen after use. Dimethylformamide (DMF) was distilled over $MgSO_4$ under reduced pressure and was stored over 4 Å molecular sieves. Toluene was purchased from Fisher and was used as received.

3.2. Fabrication of MIP samples

The sensing element of our sensor was polyurethane imprinted with anthracene following the procedure of Dickert [15,18,24]. Imprinting solutions were made by adding anthracene to the mixture of 1.25 M solutions of monomers (0.375 mmol bisphenol A and 0.455 mmol p, p'-diisocyanatodiphenylmethane) and cross-linkers (0.250 mmol trihydroxybenzene and 0.195 mmol p,o,p'-triisocyanatodiphenylmethane) in the porogen (DMF). Control solutions were prepared in a similar manner as the imprinting solution with the absence of the template anthracene. Each mixture contained a 1:1 mole ratio of hydroxy to isocyanate functional groups and a 35 mol% of cross-linking monomers.

Polymer films with various thicknesses were formed by filling identical glass vials (1.4 cm diameter) with volumes ranging from 150 to 400 μl of the freshly prepared mixtures of the imprinting or non-imprinting solutions. Since the polymer shrinks during polymerization, about 3 μl of a catalyst (tetramethylethylene diamine) was added to each polymer sample to increase the polymerization rate and to retain the initial shape of polymers. The polymerization was completed within seconds, forming a yellow polymer on the bottom of the glass vials. All the procedures were carried out at room temperature in air. MIP samples with different thicknesses (0.15, 0.22, 0.5, 1.16, 1.45, 1.76, and 2.2 mm)

and with different imprinted anthracene concentrations (0, 0.32, 0.64, 3.2, 12.8, and 25.5 mM) were synthesized.

To prepare thin films for absorbance measurements, microscope cover slips were used as spacers between two glass microscope slides. A MIP film of 150 μm was formed in the space between the glass slides. In this way, the thickness of the MIP was controlled by the height of the cover slip. Because the MIP shrank from the sides, the thickness of the MIP remained constant. To make samples for the quantum yield measurement, the polymer solution with anthracene was polymerized directly in a standard 1 cm quartz cuvette. These same samples were used to make refractive index measurements with an Abbé refractometer. After 1 day of polymerization, the MIPs shrank and could be removed from the cuvette.

3.3. Optical characterization

The absorbance of 0.15 mm thick films of control and imprinted samples were measured with a HP-8452A diode array spectrophotometer. The absorption coefficients of the MIP were obtained from the absorbance values, $\mu_a(\lambda) = A(\lambda)\ln(10)/t$, where t is the thickness of the MIP film. Since the optical properties of the polymers changed over time as the solvent evaporated, the absorption coefficients were measured daily until the solvents evaporated completely (~3 days for 0.15 mm thick samples).

The refractive index of MIP bulk samples was measured using an Abbé refractometer (model ABBE-3L). The measurement became more difficult as the polymer dried and darkened over several days. The refractive index of polyurethane bulk samples was 1.47 ± 0.01 for the first 3 days.

3.4. Quantum yield measurement

In our characterization of the single-wavelength quantum yields of anthracene in MIPs, the excitation wavelength was 358 nm, while the emission at 404 ± 1 nm of anthracene in MIPs was compared to the total emission from 368 to 550 nm of a standard solution (0.3 g/l anthracene in cyclohexane), which has a quantum yield of 0.36 [25,26]. Several conditions need to be satisfied following Parker's method [25]. First, to minimize the effect of variation in the intensity of the excitation light as a function of wavelength, we chose 358 nm as the excitation wavelength for all the measurements. Second, we assumed all the excitation photons were absorbed. We chose anthracene in cyclohexane with 0.3 g/l concentration as our standard solution based on Berlman's method [26]. At this concentration, the absorption coefficient is 31 cm^{-1}, which allows $<10^{-14}$ of light to be transmitted through the 1 cm cuvette sample ($T = \exp(-31)$), thereby ensuring all light was absorbed. The total absorption coefficient for our MIP samples was the sum of the absorption coefficient of the polymers (15 cm^{-1}) and the anthracene. This high total absorption coefficient value also ensured all light was absorbed. Third, the geometry factor of the sensing system should be the same for all the samples. The geometry factor was affected by the penetration depth of excitation light and the refractive index of solutions. Since relatively high concentrations of anthracene were used for all the measurements, the variation of penetration depth was less than 0.6 mm, for MIP samples with anthracene concentrations between 0.16 mM ($\mu_a^f = 17\ cm^{-1}$) and 25 mM ($\mu_a^f = 317\ cm^{-1}$). As for the refractive index mismatch between different solvents, an n^2 term was included in Eqs. (4) and (5) [26] below.

A spectrofluorimeter (SPEX Fluorolog model 112) was used to produce excitation light ($\lambda_x = 358 \pm 1$ nm) and to collect the emission spectra of the samples. Fluorescence of MIPs formed in quartz cuvettes and anthracene in cyclohexane were measured. Since polyurethane itself fluoresces at an excitation wavelength 358 nm, the fluorescence from anthracene is only a fraction of the total emission. In this case, the quantum yield of polyurethane at 404 ± 1 nm, $\Phi^{404}_{urethane}$, was calculated using Eq. (4) below [25]. Then, the quantum yield of anthracene in MIPs at 404 ± 1 nm, $\Phi^{404}_{anthracene}$, was calculated using the Eq. (5).

$$\Phi^{404}_{urethane} = \Phi_{std}\frac{I^{404}_{urethane}}{I^{total}_{std}}\left(\frac{n_{mip}}{n_{std}}\right)^2 \tag{4}$$

$$\frac{\mu^{404}_{anthracene}}{\mu^{404}_{anthracene}+\mu^{404}_{urethane}}\Phi^{404}_{anthracene} + \frac{\mu^{404}_{urethane}}{\mu^{404}_{anthracene}+\mu^{404}_{urethane}}\Phi^{404}_{urethane} = \Phi_{std}\frac{I^{404}_{mip}}{I^{total}_{std}}\left(\frac{n_{mip}}{n_{std}}\right)^2 \tag{5}$$

where Φ_{std} is the quantum yield of the standard solution; $I^{404}_{urethane}$ the emission of polyurethane alone at 404 ± 1 nm; I^{404}_{mip} the emission of MIPs at 404 ± 1 nm; I^{total}_{std} the total emission of the standard solution; $\mu^{404}_{urethane}$, $\mu^{404}_{anthracene}$ the absorption coefficients at 404 nm of polyurethane alone and anthracene in MIPs; and n_{std}, n_{mip} the refractive indices of the standard solution and MIPs, respectively.

3.5. Fluorescence collection efficiency measurement

The test system consisted of a glass vial (diameter = 1.4 cm, height = 5 cm) coated with a MIP as the sensing layer on its flat bottom (Fig. 2). Only a fraction G (the "geometry factor" discussed earlier) of the emitted light was collected by the system. Fluorescence was measured while anthracene was still imprinted in the polymers. Different anthracene concentrations and different thickness of MIP films (those vial samples made in Section 3.2) were tested. A mechanical fixture constrained the position of the vial samples for each measurement. This fixture was adjusted so that the 0.5 mm × 10 mm rectangular excitation beam would focus on the middle of the sample. For excitation at 358 nm, the emission spectrum was recorded from 370 to

480 nm (1 nm bandpass, 2 s/nm). The term, $I^{404}_{mip}/I^{x}_{exp}G$, in the Eq. (2) could then be calculated.

3.6. Rebinding characterization

To study the rebinding performance of the imprinted polymers, extraction of anthracene and subsequent rebinding experiments were performed. MIP samples imprinted with 25 mM anthracene were compared with non-imprinted samples.

The imprinted anthracene was removed by soaking the films in toluene. For better extraction, the samples were shaken continuously and the toluene was replaced every 2 days. The fluorescence signal of the toluene solution was used to check if imprinted anthracene had been extracted. Because the prepared vial-samples were thick, it took 2 weeks to complete most of the extraction. After extraction, the samples were placed under vacuum to remove residual solvent. The fluorescence signal of the polymer itself was then measured using the same setup in Fig. 2.

Rebinding solutions were made by dissolving anthracene in DMF. Calibration curves were derived by measuring the fluorescence intensity of different concentrations (0.01–0.22 mM) of anthracene/DMF solutions in standard quartz cuvette using a fluorimeter (Fluorolog 112). Then, 2.5 ml of 1 mM anthracene solution was added to each of the imprinted and non-imprinted polymer samples. The vials were sealed with aluminum foil and shaken for 2 days. Subsequently, the rebinding solution was diluted to 1/15 of its original concentration in a standard cuvette. The fluorescence signal was measured and the anthracene concentration was derived from the calibration curve.

4. Results

4.1. Optical characterization

Polyurethane changes its optical properties as it dries, making the definition of background absorption coefficient time dependent. Fig. 3 shows the absorption coefficients of polyurethane over 3 days.

The absorption coefficients of 1 mM anthracene in cyclohexane, DMF, and polyurethane on day 1 (the first day) are compared in Fig. 4. The absorption coefficient of anthracene in polyurethane decreased ~10% as the MIPs dried. The absorption coefficient was $5.1 \pm 0.2\,cm^{-1}$ at 358 nm on day 1. The spectrum of anthracene in polyurethane shows a 6 nm Stokes shift compared to the spectrum of anthracene in cyclohexane.

The single wavelength (404 ± 1 nm) quantum yield of polyurethane was calculated to be 0.00050 ± 0.00004. The single wavelength (404 ± 1 nm) quantum yield of anthracene in MIPs as a function of anthracene concentration is plotted in Fig. 5. As can be seen, the quantum yield decreases with increasing concentration.

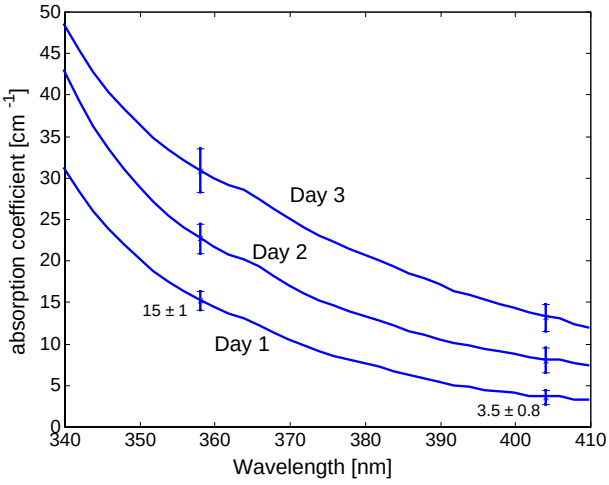

Fig. 3. The background absorption coefficients of polyurethane as a function of wavelength over 3 days. The absorption coefficient was $15 \pm 1\,cm^{-1}$ at the excitation (358 nm) wavelength of anthracene and $3.5 \pm 0.8\,cm^{-1}$ at emission (404 nm) wavelength on day 1 (the first day). The error bar is the standard deviation of 5 measurements.

4.2. Model results and experimental verification

The simulation result (right hand side of Eq. (2)) was compared with the experimental result (left hand side of Eq. (2)) in Fig. 6. Assuming that the input excitation energy is 1 J, the output fluorescence is represented as μJ. These measurements had a 14% standard deviation from the model.

To understand how the thickness of a MIP layer and the background absorption properties of MIPs affect anthracene fluorescence signals ($\Phi^{404}_{anthracene} N^{m}_{anthracene}/N^{x}_{model}$ in Eq. (2)), several other simulations were constructed. Fig. 7 shows the anthracene fluorescence energy versus the thickness of MIP films ranging from 0.01 to 1 mm and for anthracene concentrations ranging from 30 ppm to 3 ppb (assuming $\mu^{x}_{urethane} = \mu^{m}_{urethane} = 1\,cm^{-1}$, and $\Phi^{404}_{anthracene} =$

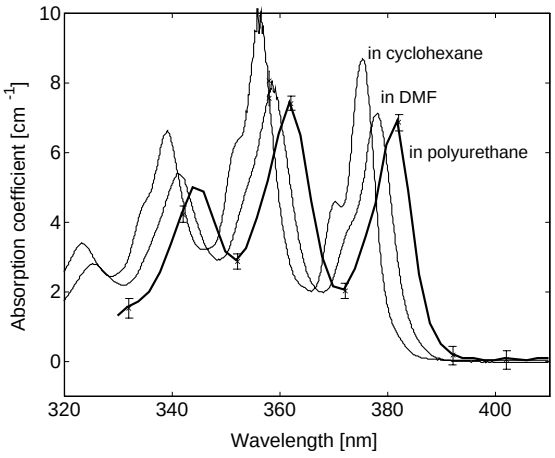

Fig. 4. Anthracene (1 mM) absorption coefficients in cyclohexane, DMF, and polyurethane. Anthracene in polyurethane showed a 6 nm stokes shift from anthracene in cyclohexane.

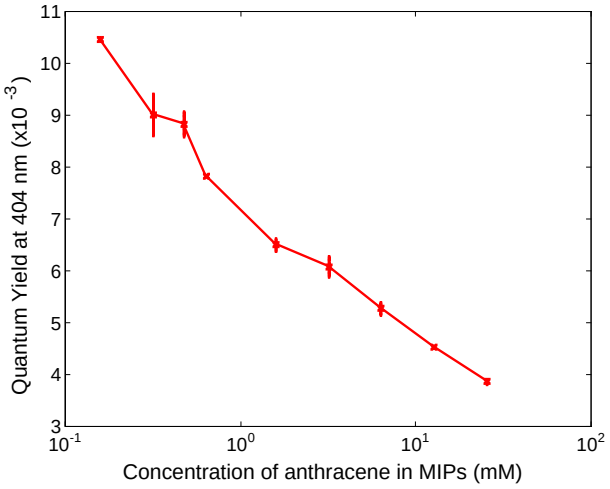

Fig. 5. The quantum yield of anthracene in MIPs at 404 ± 1 nm as a function of anthracene concentration.

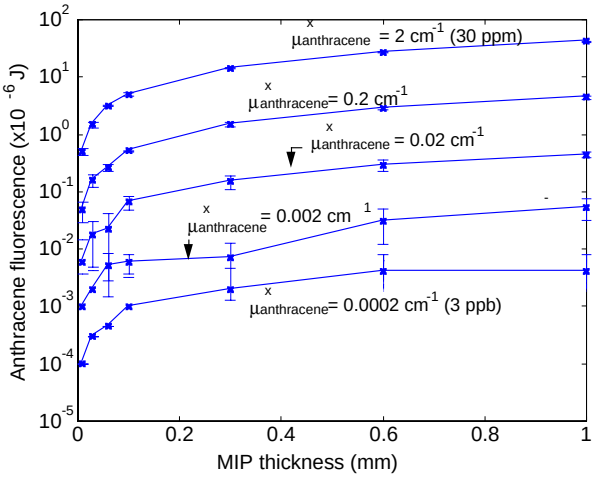

Fig. 7. Simulation result of the fluorescence emission versus MIP thickness at different anthracene concentrations for a background absorption μ_{urethane} of 1 cm^{-1} and input energy of 1 J.

0.01). Typically, a thicker sensing layer yields higher fluorescence signals. This prediction agrees with the observation of other researchers [18]. Observe that the fluorescence signal increases dramatically with thickness over 0.1 mm, and increases moderately above 0.3 mm. Also note that 3 ppb anthracene concentrations yield only 5 nJ fluorescence energy for 1 J excitation light.

Fig. 8 is a simulation of anthracene fluorescence for different background absorptions, $\mu^{\text{x}}_{\text{urethane}}$ and $\mu^{\text{m}}_{\text{urethane}}$, for four thicknesses. Note that the background absorption has greater influence on thicker MIP samples (0.5 mm and 1 mm). The fluorescence signal decreases about 50% for a 1 mm thick MIP sample and about 20% for a 0.5 mm thick sample as the background absorption increases from 1 to 10 cm^{-1}. The model also shows that the background absorption does not make much difference for thinner MIP samples (≤0.2 mm). The fluorescence signal of a 0.1 mm thick, 30 ppm fluorophore concentration sample is 5 μJ for 1 J of excitation light.

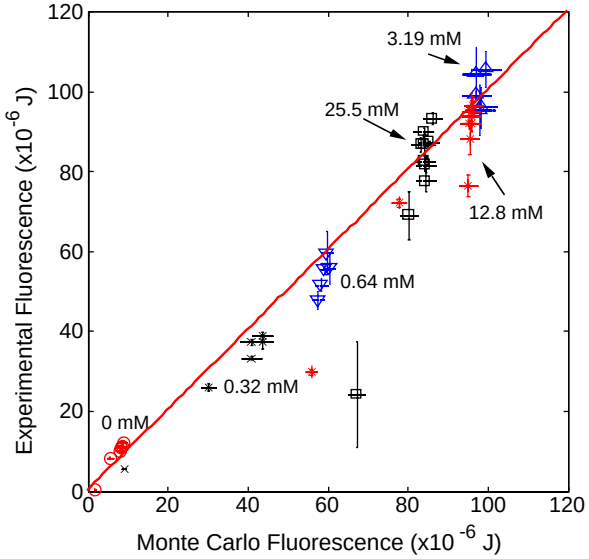

Fig. 6. The experimental results versus the Monte Carlo simulation. Error in experimental values are the standard deviation of five sample measurements. Errors in Monte Carlo values are the standard deviation of three simulations and the quantum yield. Markers with the same shape represent the same concentration group of anthracene in MIPs. For the same concentration group, each marker represents different thickness of MIP films. These measurements showed 14% standard deviation in the model.

4.3. Rebinding

Table 1 summarizes the results of rebinding study on 25 mM anthracene imprinted polymer and on non-imprinted control polymer samples. Generally, the imprinted polymers showed about six times more rebinding than the

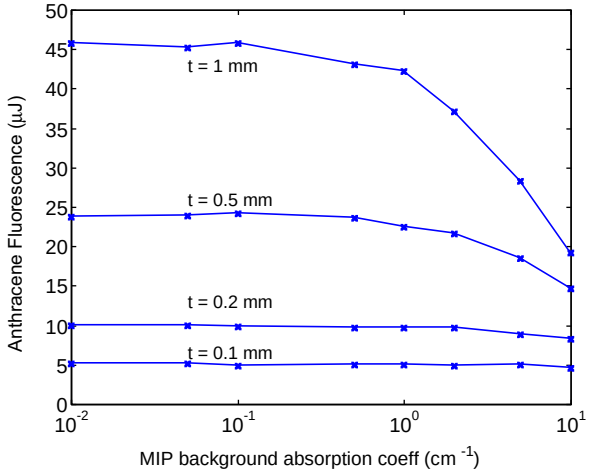

Fig. 8. Simulation result of the fluorescence emission versus MIP background absorption, $\mu^{\text{x}}_{\text{urethane}}$ and $\mu^{\text{m}}_{\text{urethane}}$, for MIP thickness = 1, 0.5, 0.2, and 0.1 mm at fluorophore concentration of 30 ppm ($\mu^{\text{x}}_{\text{anthracene}} = 2\ \text{cm}^{-1}$).

Table 1
Results of rebinding study

MIP sample (#)	MIP volume (μl)	Fluorescent signal before rebinding (A.U.)	Bound concentration (ppm)	Molecule bound density (μmole/g)	Bound % of theoretical imprinted sites (%)
Ca	400	420 ± 8	4.2 ± 0.4	0.18 ± 0.02	
Cb	350	430 ± 20	3.5 ± 0.3	0.17 ± 0.01	
Cc	300	430 ± 20	2.4 ± 0.2	0.14 ± 0.01	
Cd	250	440 ± 20	1.7 ± 0.1	0.12 ± 0.01	
Ce	200	400 ± 20	1.7 ± 0.1	0.15 ± 0.01	
Cf	150	370 ± 10	1.9 ± 0.1	0.23 ± 0.01	
A4a	400	500 ± 30	28.6 ± 0.8	1.23 ± 0.03	3.7 ± 0.1
A4b	350	1070 ± 20	13.4 ± 0.2	0.66 ± 0.01	2.0 ± 0.03
A4c	300	1890 ± 60	[a]	–	–
A4d	250	360 ± 20	17.4 ± 0.3	1.19 ± 0.02	3.6 ± 0.05
A4e	200	320 ± 5	15.2 ± 0.6	1.30 ± 0.05	3.9 ± 0.2
A4f	150	300 ± 6	12.4 ± 0.4	1.42 ± 0.04	4.3 ± 0.1

A4a–A4f represent 4 mol% imprinted polymers, while Ca–Cf represent non-imprinted polymers. The third column is the fluorescence signals from the MIP layer detected after extraction but before rebinding. All the errors are the standard deviation of four concentration measurements.

[a] The concentration of rebinding solution forA4c sample was 1.66 mM after rebinding test, which was higher than the starting concentration 1 mM. This is because the anthracene molecules were not extracted completely before the rebinding, which also agreed with the strong fluorescence signals (1890) from the MIP layer before rebinding.

non-imprinted control polymers. Note that samples A4b and A4c still exhibited fluorescence at 404 nm after 2 weeks of extraction. These two samples did not have the templated analytes extracted completely because the MIPs were stuck to the bottom of the vials. Consequently, A4b only rebound 0.66 ± 0.01 μmol/g, while A4c would have had a negative rebinding density (because residual anthracene in the MIP would be extracted by the rebinding test solution).

5. Discussion

The quantum yield of anthracene in MIPs decreases as the concentration of anthracene increases from 0.1 to 25 mM. This result is possibly due to the aggregation of anthracene molecules since the concentrations we used were relatively high [15,27–29]. A similar result was found in Rhodamine 6G and Rhodamine B at concentrations greater than 0.05 mM by Bindhu et al. [27,28]. Dickert et al. also observed that a linear relationship between the fluorescence emission and the analyte (polycyclic aromatic hydrocarbon (PAH)) concentration was only valid when the quantum yield did not change with increasing analyte concentration (up to several $\mu g l^{-1}$) in the MIP layer [29]. To check if this condition occurs in a different medium, we measured the quantum yield of anthracene in DMF. The result showed a fairly constant quantum yield when anthracene concentration ranged from 0.05 to 0.8 mM. As the concentration increased, the quantum yield decreased quickly. Moreover, the quantum yield of another fluorescent molecule, 7-carboxymethoxy-4-methyl-coumarin (in methanol), was also measured as a comparison. The quantum yield remained constant in the concentration range of 0.02–0.5 mM. Above 0.5 mM, the quantum yield of coumarin decreased. Another possible explanation is that the absorption coefficient may be responsible for the decrease in anthracene fluorescence and therefore lower apparent quantum yields. However, the absorption coefficient did not change over the concentration ranges from 0.1 to 25.5 mM.

The rebinding performance of MIPs was examined. The results of rebinding study (Table 1) showed that the binding capacity was ∼1.2 μmol/g (about 180 ppm in MIP) for the 4 mol% imprinted polymers, while nonspecific binding was ∼0.15 μmol/g for non-imprinted polymers. Although the overall rebinding capacity was moderate [30,31], the imprinted polymers bound six times more than the non-imprinted polymers, indicating an imprinting effect that was comparable with other published studies [18,19,32]. Dickert et al. [18,19] had about 100 times greater response from anthracene-imprinted polyurethane than control samples. One possible reason for our relatively low binding capacity was that polymer films we fabricated were much thicker (≥100 μm) than those prepared by Dickert (several microns). Since the rebinding of analyte molecules to the recognition sites is diffusion controlled [33], the molecules may not be able to access the sites that are buried inside the highly cross-linked polymer matrix. It is possible that only those imprinted cavities on the outer layer of the polymers were bound. However, we did not use thinner MIP films for two reasons: (1) thin films broke and had inconsistent thicknesseses, and (2) thinner MIP films have correspondingly weak fluorescence signals as shown in Fig. 7. The number of fluorescent analytes trapped by a MIP can be monitored either from the loss of the fluorescence of the analyte solution or from the increase of the analyte fluorescence of the MIP. Detecting the fluorescence signals directly from the MIPs instead of the solution provides a convenient way to follow either extraction or rebinding of

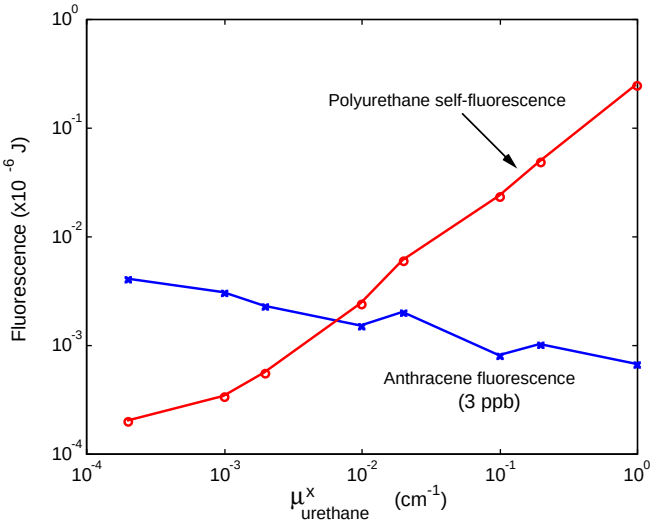

Fig. 9. Simulation of the fluorescence emission at 404 ± 1 nm from polyurethane, and anthracene versus polyurethane absorption coefficient $\mu^{x}_{urethane}$ at excitation wavelength 358 nm.

analytes. The following parameters affect the sensitivity of this type of MIP sensors: (1) the thickness of a MIP sensing layer, (2) the background absorption of excitation light, and (3) the fluorescence yield of the polymers. According to our model (Fig. 7), a 0.2 mm thick film will maximize fluorescence signals, and the background absorption of excitation light by the polymers, $\mu^{x}_{urethane}$, needs to be reduced. Although our model shows that $\mu^{x}_{urethane}$ does not have strong influence on the fluorescence emission from a 0.2 mm thick MIP (Fig. 8), high $\mu^{x}_{urethane}$ will increase the polymer self-fluorescence emission.

To further examine the effect of polymer background absorption on the fluorescence signals ($\Phi^{404}_{anthracene}N^{m}_{anthracene}/N^{x}_{model}$, and $\Phi^{404}_{urethane}N^{m}_{urethane}/N^{x}_{model}$ in Eq. (2)), another simulation was constructed as shown in Fig. 9. In this simulation, the MIP thickness was 0.2 mm, the anthracene absorption coefficient $\mu^{x}_{anthracene}$ was 0.0002 cm^{-1}, the polyurethane absorption coefficient at emission wavelength $\mu^{m}_{urethane}$ was 1 cm^{-1}, and quantum yields, $\Phi^{404}_{urethane}$, and $\Phi^{404}_{anthracene}$, were 5×10^{-4}, and 0.01 respectively. Notice that as the absorption coefficient, $\mu^{x}_{urethane}$, increased from 0.0002 to 1 cm^{-1}, the anthracene fluorescence decreased 10 times; in contrast, the polymer fluorescence increased more than 1000 times. Also, note that when $\mu^{x}_{urethane}$ is greater than 0.005 cm^{-1}, the polyurethane self-fluorescence exceeds the anthracene fluorescence. This suggests that to detect 3 ppb anthracene concentration with signal (anthracene fluorescence) to noise (polymer fluorescence) ratio of 10:1, polymer should have an absorption coefficient less than 0.001 cm^{-1} (assuming the quantum yields remain the same over the concentration ranges). An alternative is to imprint a different PAH molecule that fluoresces at longer wavelengths to minimize the background absorption and emission by the polymers. Tetracene has fluorescence ranging from 480 to 580 nm, yet polyurethane still has absorption up to 0.5 cm^{-1} at 550 nm and has fluorescence emission at this wavelength range as well. An additional problem with imprinting tetracene was that the imprinting capacity of this molecule was lower than that of imprinting with anthracene due to the lower solubility of tetracene in DMF. Alternatively, reducing the quantum yield of polymer can decrease the noise from polymer self-fluorescence. According to Fig. 9, polymers have about 5000 times fluorescence signal of anathracene at $\mu^{x}_{urethane} = 1\,cm^{-1}$. To reach a signal-to-noise ratio of 10:1, the quantum yield of the polymer must be reduced by a factor of 50,000 assuming $\mu^{x}_{anthracene}$ remains constant. This means the ratio of the quantum yield of fluorescence analyte to the quantum yield of polymers at the detection wavelength needs to be about 100,000.

Although our model shows that this particular polyurethane imprinted system may not be optimal for optical sensors, polyurethane can be incorporated with a quartz crystal microbalance (QCM) device for better quantitative measurements as originally studied by the Dickert and Tortschanoff [15]. To optimize a fluorescence-based MIP sensor, one should use polymers that have lower background absorption and fluorescence emission.

6. Conclusions

We have developed a theoretical model for the fluorescence collection efficiency of a MIP sensor that consists of a MIP sensing layer on a transparent substrate. This model may be used to analyze the sensitivity and detection limit of an optical system and to provide an optimization strategy for the sensor design. This simulation method can be modified easily to accommodate various optical sensor designs. We have evaluated one MIP design by varying the thickness of MIP sensing layers, background absorptions, background fluorescence, and rebinding performance. We found that thicker MIP sensing layers tend to be more sensitive. To improve signal-to-noise, both background polymer absorption and fluorescence need to be reduced. Our model may be used to improve the sensitivity of other sensor designs.

Acknowledgements

This work was supported by the National Institute of Health under Grant NIH-CI-R24-CA84587-03. We thank Dr. Wamser at Department of Chemistry, PSU for use of his fluorimeter.

References

[1] R.C. Jorgenson, S.S. Yee, A fiber-optic chemical sensor based on surface-plasmon resonance, Sens. Actuators B: Chem. 12 (1993) 213–220.

[2] S. Kubitschko, J. Spinke, T. Bruckner, S. Pohl, N. Oranth, Sensitivity enhancement of optical immunosensors with nanoparticles, Anal. Biochem. 253 (1) (1997) 112–122.
[3] L. Lyon, M. Musick, M. Natan, Colloidal Au-enhanced surface plasmon resonance immunosensing, Anal. Chem. 70 (1998) 5177–5183.
[4] T.E. Plowman, J.D. Durstchi, H.K. Wang, D.A. Christensen, J.N. Herron, W.M. Reichert, Multiple-analyte fluoroimmunoassay using an integrated optical waveguide sensor, Anal. Chem. 71 (1999) 4344–4352.
[5] B.H. Schneider, E.L. Dickinson, M.D. Vach, J.V. Hoijer, L.V. Howard, Optical chip immunoassay for hCG in human whole blood, Biosens. Bioelectron. 15 (2000) 597–604.
[6] S. Subrahmanyam, S.A. Piletsky, A.P.F. Turner, Application of natural receptors in sensors and assays, Anal. Chem. 74 (2002) 3942–3951.
[7] B.M. Paddle, Biosensors for chemical and biological agents of defence interest, Biosens. Bioelectron. 11 (1996) 1079–1113.
[8] R.R. Seigel, P. Harder, R. Dahint, M. Grunze, F. Josse, M. Mrksich, G.M. Whitesides, On-line detection of nonspecific protein adsorption at artificial surfaces, Anal. Chem. 69 (1997) 3321–3328.
[9] K. Haupt, K. Mosbach, Molecularly imprinted polymers and their use in biomimetic sensors, Chem. Rev. 100 (2000) 2495–2504.
[10] M.D. Marazuela, M.C. Moreno Bondi, Fiber-optic biosensors—an overview, Anal. Bioanal. Chem. 372 (5-6) (2002) 664–682.
[11] D. Kriz, O. Ramstrom, K. Mosbach, Molecular imprinting—new possibilities for sensor technology. Anal. Chem. 69 (1997) A345-A349.
[12] L. Sabourin, R.J. Ansell, K. Mosbach, I.A. Nicholls, Molecularly imprinted polymer combinatorial libraries for multiple simultaneous chiral separations, Anal. Commun. 35 (1998) 285–287.
[13] A.L. Jenkins, O.M. Uy, G.M. Murray, Polymer-based lanthanide luminescent sensor for detection of the hydrolysis product of the nerve agent soman in water, Anal. Chem. 71 (1999) 373–378.
[14] E.H.M. Koster, C. Crescenzi, W. den Hoedt, K. Ensing, G.J. de Jong, Fibers coated with molecularly imprinted polymers for solid-phase microextraction, Anal. Chem. 10 (1995) 927–928.
[15] F.L. Dickert, M. Tortschanoff, Molecularly imprinted sensor layers for the detection of polycyclic aromatic hydrocarbons in water, Anal. Chem. 71 (1999) 4559–4563.
[16] A. Kugimiya, T. Takeuchi, Surface plasmon resonance sensor using molecularly imprinted polymer for detection of sialic acid, Biosens. Bioelectron. 16 (2001) 1059–1062.
[17] F.L. Dickert, O.Hayden, K.P. Halikias, Synthetic receptors as sensor coatings for molecules and living cells, Analyst 126 (2001) 766–771.
[18] F.L. Dickert, H. Besenbock, M. Tortschanoff, Molecular imprinting through van der Waals interactions: Fluorescence detection of PAHs in water, Adv. Mater. 10 (1998) 149–152.
[19] F.L. Dickert, P. Lieberzeit, M. Tortschanoff, Molecular imprints as artificial antibodies—a new generation of chemical sensors, Sens. Actuators B: Chem. 65 (2000) 186–189.
[20] T.E. Plowman, S.S. Saavreda, W.M. Reichert, Planar integrated optical methods for examining thin films and their surface adlayers, Biomaterials 19 (1998) 341–355.
[21] H.P. Lehr, A. Brandengurg, G. Sulz, Modeling and experimental verification of the performance of TIRF-sensing systems for oligonucleotide microarrays based on bulk and integrated optical planar waveguides, Sens. Actuators B: Chem. 92 (2003) 303–314.
[22] M.N. Armenise, V.M.N. Passaro, F.D. Leonardis, M. Armenise, Modeling and design of a novel miniaturized integrated optical sensor for gyroscope systems, J. Lightwave Technol. 19 (2001) 1476–1494.
[23] E. Hecht, Optics, Addison-Wesley, Longman Inc., New York, 1998.
[24] J.J. Brazier, M. Yan, S.A. Prahl, Y.-C. Chen, Molecularly imprinted polymers used as optical waveguides for the detection of fluorescent analytes, in: K.J. Shea, M.J. Roberts, M. Yan (Eds.), Molecularly Imprinted Materials Sensors and Other Devices, Materials Research Society Symposium Proceedings, vol. 723, 2002, pp. 115–120.
[25] C.A. Parker, Photoluminescence of Solutions, Elsevier Publishing Company, New York, 1968.
[26] I.B. Berlman, Handbook of Fluorescence Spectra of Aromatic Molecules, Academic Press Inc., New York, London, 1971.
[27] C.V. Bindhu, S.S. Harilal, V. Nampoori, C. Vallabhan, Solvent effect on absolute fluorescence quantum yield of Rhodamine 6G determined using transient thermal lens technique, Mod. Phys. Lett. B 13 (1999) 563–576.
[28] C.V. Bindhu, S.S. Harilal, Effect of the excitation source on the quantum-yield measurements of Rhodamine B laser dye studied using thermal-lens technique, Anal. Sci. 17 (2001) 141–144.
[29] F.L. Dickert, P. Achatz, K.P. Halikias, Double molecular imprinting—a new sensor concept for improving selectivity in the detection of polycyclic aromatic hydrocarbons (PAHs) in water, Fresenius J. Anal. Chem. 371 (2001) 11–15.
[30] R.J. Umpleby II, S.C. Baxter, Y.Z. Chen, R.N. Shah, K.D. Shimizu, Characterization of molecularly imprinted polymers with the Langmuir–Freundlich isotherm, Anal. Chem. 73 (2001) 4584–4591.
[31] R.J. Umpleby II, S.C. Baxter, M. Bode, J.K. Berch, R.N. Shah, K.D. Shimizu, Application of the Freundlich adsorption isotherm in the characterization of molecularly imprinted polymers, Anal. Chim. Acta 435 (2001) 35–42.
[32] E. Yilmaz, K. Mosbach, K. Haupt, Influence of functional and cross-linking monomers and the amount of template on the performance of molecularly imprinted polymers in binding assays, Anal. Commun. 36 (1999) 167–170.
[33] F.L. Dickert, O. Hayden, Molecular fingerprints using imprinting techniques, Adv. Mater. 14 (2000) 311–314.

Biographies

Yin-Chu Chen received the B.S. degree in Physics and M.S. degree in Electrical Engineering from the National Taiwan University, Taipei, Taiwan in 1995 and 1998. She is currently pursuing a Ph.D. degree in Biomedical Engineering at Oregon Health & Science University, Portland, OR. She is working with Prof. Prahl and Prof. Yan on optical molecularly imprinted polymer sensors. Her research interests include biochemical sensors, molecularly imprinted polymers, interferometry, material science, and fluorescence spectroscopy.

Jennifer J. Brazier received her B.S. degree in Chemistry and Physics from Alma College, MI in 1994 and M.S. degree in chemistry from Portland State University in 2003. Her area of research is material science of molecularly imprinted polymers.

Mingdi Yan received her B.S. degree in Materials Science and Engineering from University of Science and Technology of China, Hefei, Anhui, PR China in 1988 and Ph.D. degree in Chemistry from the University of Oregon, Eugene, OR in 1994. She is currently an Assistant Professor of Chemitry at the Portland State University. Her area of research is synthesis and microfabrication of organic and polymeric materials capable of molecular recognition.

Paulo R. Bargo received the B.S. degree in electrical engineering from the National Institute of Telecommunications, Santa Rita do Sapucai, Brazil in 1992 and the M.S. degree in electrical engineering from the University Vale do Paraiba, Sao Jose dos Campos, Brazil, in 1995. He was a visiting student at G.R. Harrison Spectroscopy Laboratory, MIT, Cambridge, MA, 1995–1996 and assistant professor at University Vale do Paraiba, 1996–1998. He just received his Ph.D. in electrical & computer engineering from the Oregon Health & Science University, Portland, OR in 2003. His research interests include optical fiber instrumentation, biological tissue spectroscopy, optical diagnostics and photodynamic therapy.

Scott A. Prahl received the B.S. degree in applied physics from the California Institute of Technology, Pasadena, CA in 1982 and the Ph.D.

in biomedical engineering from the University of Texas at Austin in 1988. He is currently a senior scientist at the Oregon Medical Laser Center of Providence St. Vincent Medical Center in Portland, OR. He is also an Assistant Professor of Biomedical Engineering in the OGI School of Science and Engineering at the Oregon Health & Science University. His current research interests include photon migration, laser thrombolysis for stroke, molecularly imprinted polymers, and coagulation techniques for hemostasis during liver surgery.